Acta Pharmaceutica Sinica B 2026;16(4):2317−2331

Chinese Pharmaceutical Association
Institute of Materia Medica, Chinese Academy of Medical Sciences

Acta Pharmaceutica Sinica B

www.elsevier.com/locate/apsb
www.sciencedirect.com

ORIGINAL ARTICLE

Isoalantolactone induces AML pyroptosis and potentiates α-PD-1 efficacy by targeting selenoprotein TXNRD1

Xiaoxuan Yu[a,b,*,†], Yanyu Zhou[a,†], Shibo Sun[c], Lu Tang[a], Wan Zhang[a], Jianqiang Xu[c,*], Wukun Liu[a,*]

[a]*Jiangsu Collaborative Innovation Center of Chinese Medicinal Resources Industrialization, School of Medicine, Nanjing University of Chinese Medicine, Nanjing 210023, China*
[b]*State Key Laboratory of Pharmaceutical Biotechnology, School of Life Sciences, Nanjing University, Nanjing 210023, China*
[c]*School of Chemical Engineering, Ocean Technology and Life Science (CEOTLS) & Panjin Institute of Industrial Technology (PIIT), Dalian University of Technology, Panjin 124221, China*

Received 3 August 2025; received in revised form 18 September 2025; accepted 7 October 2025

KEY WORDS

Isoalantolactone;
Acute myeloid leukemia;
Pyroptosis;
TXNRD1

Abstract The suppressive microenvironment of AML limits anti-PD-1 efficacy, making pyroptosis induction a key strategy for its remodeling. Isoalantolactone (IAL), a naturally occurring small molecule, has been identified herein to inhibit cytosolic thioredoxin reductase1 (TXNRD1) and trigger pyroptosis in AML cells, thereby enhancing the efficacy of anti-PD-1 antibody therapy. Mechanistically, the α,β-unsaturated carbonyl group of IAL covalently bound to the selenocysteine residue at the position 498 (Sec^{498}) of TXNRD1 through a Michael addition reaction. Clinical sample analysis revealed that TXNRD1 is overexpressed in AML, which correlates with poor prognosis. Additionally, we found that the TXNRD inhibitor auranofin has demonstrated good efficacy against AML. The inhibition of TXNRD1 activates the transcription factor peroxisome proliferator-activated receptor gamma (PPARγ), which, in turn, upregulates the transcription of caspase-3, subsequently increasing the cleavage of gasdermin E to induce pyroptosis *via* the non-classical pathway in AML cells. Additionally, enhanced caspase-3 activity promotes poly ADP-ribose polymerase 1 (PARP-1) cleavage and upregulates PD-L1 expression, thereby increasing sensitivity to anti-PD-1 monoclonal antibodies. Overall, the current study highlights a promising approach for augmenting therapy using anti-PD-1 monoclonal antibodies in AML by targeting TXNRD1 to induce pyroptosis and ameliorate the immunosuppressive microenvironment.

*Corresponding authors.
E-mail addresses: xxyu@njucm.edu.cn (Xiaoxuan Yu), jianqiang.xu@dlut.edu.cn (Jianqiang Xu), liuwukun0000@njucm.edu.cn (Wukun Liu).
†These authors contributed equally to this work.

Peer review under the responsibility of Chinese Pharmaceutical Association and Institute of Materia Medica, Chinese Academy of Medical Sciences.

https://doi.org/10.1016/j.apsb.2025.12.040

1. Introduction

Acute myeloid leukemia (AML) is the most challenging subtype of leukemia, and remains the deadliest hematologic malignancy with high morbidity and severe mortality annually[1,2]. Despite advances in treatment paradigms, AML remains a formidable therapeutic challenge. The conventional "7 + 3" backbone, though foundational, is hampered by dose-limiting toxicities[3]. Recent advances in precision medicine—including BCL-2, FLT3 and IDH1/2 inhibitors—have demonstrated selective efficacy in genetically stratified cohorts[4-7]. Nevertheless, emerging immunotherapies exhibit antitumor potential but remain constrained by immune-mediated adverse events[8]. AML fosters an immunosuppressive milieu marked by diminished apoptosis and pyroptosis, accompanied by attenuated inflammatory cytokine production such as IFN-γ, IL-6 and TNF-α[9-12]. This immunosuppression is further exacerbated by exhausted effector T/NK cells, dysfunctional dendritic cells (DCs)[13,14], and expanded immunosuppressive populations[10,15].

The immune checkpoint play a pivotal role in AML immune evasion by sustaining an immunosuppressive microenvironment[16,17]. While checkpoint blockade has transformed cancer therapy, its efficacy in AML, particularly targeting PD-1/PD-L1 remains limited[18-20]. Combining PD-1/PD-L1 inhibitors with demethylating agents or chemotherapy has yet to show significant clinical benefit, likely due to the intricate heterogeneity of the AML immune landscape[18,21,22,19,23]. Identifying common therapeutic targets in both AML cells and their microenvironment may help overcome these challenges.

Redox homeostasis constitutes a fundamental pillar of cellular integrity, with the thioredoxin reductase (TXNRD) family serving as master regulators of this delicate equilibrium[24]. Of particular oncological significance, malignant cells frequently exploit TXNRD1 overexpression as an evolutionary conserved survival strategy, establishing a redox buffer system that orchestrates reactive oxygen species (ROS) neutralization while amplifying endogenous antioxidant capacity[25]. This redox regulatory network intersects critically with pyroptotic pathways—a specialized inflammatory cell death program mediated through inflammasome activation and caspase cascades[26]. Mechanistic studies reveal TXNRD1's redox-sensitive modulation of thioredoxin 1 (TXN1) serves as a critical checkpoint for caspase-11 activation, particularly under septic conditions[27]. The therapeutic implications for AML are profound: pyroptosis-induced cytokine storms may effectively counteract the immunosuppressive tumor niche, creating immunological synergy with PD-1 blockade[28-30]. Crucially, while AML exhibits marked interpatient heterogeneity, the near-universal presence of TXNRD1 dysregulation and associated oxidative stress across subtypes identifies this pathway as a compelling therapeutic node[31].

Isoalantolactone (IAL), a sesquiterpene lactone derived from *Inula helenium* L. (commonly known as Tu-Mu-Xiang in Chinese), has been shown to possess significant antitumor properties, with demonstrated inhibitory effects against various types of cancer, including hepatocellular carcinoma[32], ovarian carcinoma[33], melanoma[34], chronic myeloid leukemia (CML)[35], and breast cancer[36]. However, its role in inducing pyroptosis in AML cells and modulating the immune response in AML remains unclear. The previously demonstrated anticancer mechanisms of IAL include, but are not limited to, the inhibition of p38/mitogen-activated protein kinase (MAPK)/nuclear factor kappa-light-chain-enhancer of activated B-cells (NF-κB) signaling pathway[36], induction of ROS-mediated endoplasmic reticulum (ER) stress[37], suppression of the signal transducer and activator of transcription 3 (STAT3) signaling pathway[37], and inhibition of the AKT/mammalian target of rapamycin (mTOR) pathway[34,38]. These pathways are critically involved in AML pathogenesis: constitutive NF-κB activation sustains chemoresistance *via* anti-apoptotic proteins and pro-inflammatory cytokines[39]; STAT3 modulates the immunosuppressive microenvironment in chronic lymphocytic leukemia (CLL) by suppressing regulatory B-cell (Breg) functions and inhibiting the PD-1/PD-L1 axis[40]. Separately, the AKT/mTOR pathway supports leukemic cell survival through metabolic adaptations such as oxidative phosphorylation[41]. Despite these findings, the direct molecular targets of IAL have not been entirely elucidated.

In this study, we investigated the antileukemic activity of IAL both *in vitro* and *in vivo*, and demonstrated its ability to induce pyroptosis in AML cells and enhanced the efficacy of anti-PD-1 therapy. We found that IAL may directly target the C-terminal redox-active Sec^{498} of TXNRD1 and inhibit the enzymatic activity. The TXNRD1 inhibition leads to the activation and nuclear translocation of peroxisome proliferator-activated receptor gamma (PPARγ). These findings in the current study show that IAL not only exerts potent antitumor activity but also modulates the immune microenvironment in AML, throwing valuable insights on potential clinical application of IAL in AML treatment.

2. Materials and methods

2.1. Reagents and antibodies

The IAL was purchased from Shanghai yuanye Bio-Technology Co., Ltd. (China). Fluorescently labeled antibodies-FITC-conjugated anti-human CD45 (cat. no. MHCD4501) was procured from Thermo Fisher Scientific (United States). The TXNRD1 Activity Assay Kit and the ROS Assay Kit (DCFH-DA, product ID 3130) were obtained from Solarbio Corp. (Beijing, China).

2.2. Cell culture and patient samples

The human AML cell line THP-1 was acquired from the Cell Bank of the Shanghai Institute of Biochemistry and Cell Biology (Shanghai, China). Cells were grown in suspension using RPMI-1640 medium (GIBCO, USA), supplemented with 10% fetal bovine serum (FBS, Life-iLab, China) and 100 U/mL penicillin—streptomycin. All cultures were incubated at 37 °C in a humidified atmosphere containing 5% CO_2. The murine AML cell

line C1498 was sourced from Fenghui Biotechnology Co., Ltd. (Changsha, China). Primary leukemic cells were isolated from AML patients at Jiangsu Province Hospital (Nanjing, China) using lymphocyte-monocyte separation medium (Jingmei, Shanghai, China).

2.3. Lentiviral transduction of the hyper sensor

For transduction experiments, THP-1 cells were seeded at a density of 5×10^4 cells per well and transduced with different Hyper variants for 48 h prior to the addition of accessory reagents A and B (41102ES10, YEASEN). Transfection efficiency was verified to be optimal at an MOI of 100. To assess H_2O_2 signaling across Hyper variants with or without AF treatment, all samples were analyzed using both a Leica SP8 confocal laser scanning microscope (Germany) and flow cytometry. The resulting Hyper signal datasets were processed and analyzed using FlowJo (version 10.8.1).

2.4. Mouse tumor model and treatment regimens

2.4.1. Patient-derived xenograft model

Female NOD/SCID mice, aged 6−8 weeks, were subjected to sublethal irradiation (1.8 Gy) and inoculated with 1×10^7 human primary AML cells per mouse *via* tail vein injection within 24 h post-irradiation. After 7 days, the mice were administered IAL (30 mg/kg), AF (5 mg/kg), and DOX (1.25 mg/kg) by intraperitoneal injection every other day for two weeks. A control group received equivalent volumes of normal saline to evaluate the effect of treatment administration on survival. Animals were monitored daily for an additional 4-week period. Peripheral blood, bone marrow, and splenic cells were harvested and stained with an anti-human CD45 antibody for flow cytometric analysis.

2.4.2. Allograft AML model

To establish an AML model, C57BL/6 mice were intravenously injected with Luciferase-C1498 cells at a dose of 5×10^6 cells per mouse *via* the tail vein. On Day 7 post-inoculation, the mice were randomly assigned to four treatment groups receiving IAL (30 mg/kg), AF (5 mg/kg), DOX (1.25 mg/kg), or normal saline. Bioluminescence imaging was performed on Days 10, 20, and 30 to monitor disease progression. Tissue samples collected on Day 25 were fixed in 4% paraformaldehyde and processed into sections using standard protocols. Sections of 4 μm thickness were prepared, dewaxed, and subjected to antigen retrieval. Immunohistochemical staining was carried out using primary antibodies against CD4, CD8, and Gr-1, along with corresponding HRP-conjugated secondary antibodies. Images were acquired using a light microscope.

2.4.3. Cell-derived xenograft model

C1498 cells (5×10^6 cells/mouse) were subcutaneously inoculated into C57BL/6 mice. On Day 7, the animals were randomly allocated into three experimental groups and administered with IAL (30 mg/kg), AF (5 mg/kg), or normal saline, respectively. Two weeks after treatment initiation, all mice were humanely euthanized, and the resulting tumors were dissected for assessment of both mass and dimensions. Protein extracts from tumor tissues were subsequently prepared for evaluation of target protein expression levels.

2.5. RNA sequencing (RNA-seq)

THP-1 cells were seeded in 10-cm culture dishes and exposed to AF for 24 h. Following incubation, the cells were lysed and the resulting lysates were subjected to centrifugation. Total RNA was isolated using Trizol™ reagent (Yeasen, China). The purified RNA samples were subsequently delivered to Shanghai Majorbio BioPhamtech Corporation for RNA sequencing. Subsequent bioinformatic analyses were performed utilizing the Majorbio Cloud Platform (https://cloud.majorbio.com).

2.6. Western blot analysis

THP-1 cells were seeded in a 6-well plate and treated with IAL for 24 h. Cells were washed with cold PBS twice, then resuspensed with RIPA buffer (89901, ThermoFisher). The protein concentration in cell lysates was quantified with a BCA Protein Assay Kit (23227, ThermoFisher). Enhanced chemiluminescence (ECL) immunodetection was carried out with a commercial system (36222ES60, YEASEN). The following antibodies were sourced from respective suppliers: GADPH (D16H11, CST), Caspase-3 (A11319, Abclonal), cleave-Caspase-3 (ab198447, abcam), PPARα (A6697, Abclonal), PPARβ (orb1089300, Biorbyt), PPARγ (A0270, Abclonal), GSDME (ab215191, Abcam), and PD-L1 (A19135, Abclonal).

2.7. Reduction of IAL

After dissolving the IAL and cuprous chloride in methanol, sodium borohydride was added in a molar ratio of IAL:sodium borohydride:cuprous chloride = 5:12.5:3, and the reaction yielded the reduced IAL.

2.8. ROS detection

Human AML cells were incubated with IAL at different concentrations (10, 20, and 40 μmol/L) for 3 h. After washing with PBS, cells were applied with 10 μmol/L 2′,7′-dichlorofluorescein diacetate (DCFH-DA) at 37 °C in the dark for 25 min. ROS generation was measured according to the increase of fluorescence signals at $Em_{520\ nm}/Ex_{488\ nm}$ by using a fluorescent microscopy (Leica DMi8, Germany).

2.9. TXNRD1 enzyme activity assay

The catalytic function of recombinant rat TXNRD1 was assessed through a conventional DTNB reduction assay[42]. Wild-type TXNRD1 was tested at a concentration of 10 nmol/L, while mutant variants were assessed at 100 nmol/L. The mutant variants were assayed at 100 nmol/L due to their relatively lower enzymatic activity. The reaction mixture consisted of 2.5 mmol/L DTNB and 300 μmol/L NADPH in TE buffer (pH 7.5). Absorbance readings at 412 nm, reflecting the generation of TNB anions, were recorded to monitor enzymatic activity using a SpectraMax ABS microplate reader (Molecular Devices, USA).

2.10. Isothermal titration calorimetry (ITC) assay

The binding affinity between IAL and TXNRD1 was measured using NANO ITC. Purified TXNRD1 (5 μmol/L) was loaded into the sample cell, and IAL was titrated into the cell in 19 successive

injections (2 μL per injection) at 25 °C. The dissociation constant (K_d) was calculated using a one-site binding model.

2.11. Removal of unbound IAL by desalting

Recombinant TXNRD1 was initially reduced with 100 μmol/L NADPH for 10 min at room temperature. The reduced enzyme was subsequently treated with IAL, and unbound compound was eliminated *via* a NAP-5™ desalting column (Cytiva™, Uppsala, Sweden). Enzymatic activity of the desalted TXNRD1 was then assessed using a standard DTNB reduction assay.

2.12. LC−MS analysis of IAL-GSH adducts

To analyze the interaction between IAL and GSH, 100 μmol/L IAL was incubated with 1 mmol/L reduced form of glutathione (GSH) for 12 h. The resulting adducts were separated by using a Hypersil GOLD™ C18 column (100 mm × 2.1 mm, 3 μm, ThermoFisher Scientific, USA) in a reverse-phase chromatography (RP-HPLC). Elution was achieved with a gradient of 2% to 95% (*v*/*v*) acetonitrile in 0.1% (*v*/*v*) formic acid at a flow rate of 0.4 mL/min over 10 min. Mass spectra of IAL-GSH adducts were recorded using a UPLC-Q-Exactive Orbitrap MS (Thermo Fisher, USA) with a full scan ranging from 200 to 2500 *m*/*z* at a resolution of 70,000[43].

2.13. LC−MS/MS analysis of IAL targeting site(s) on TXNRD1

Pre-reduced TXNRD1 (2 μmol/L), treated with NADPH, was incubated with 200 μmol/L IAL for 4 h at room temperature. The mixture was desalted *via* NAP-5™ columns (Cytiva, Uppsala, Sweden) and lyophilized. The resulting protein powders were resuspended in 50 mmol/L ammonium bicarbonate buffer containing 8 mol/L urea. Reduction was performed with 20 mmol/L DTT at 65 °C for 1 h, followed by alkylation of newly generated thiol groups using 40 mmol/L iodoacetic acid (IAA) under dark conditions at room temperature for 30 min. The alkylation reaction was terminated by adding 10 mmol/L DTT. After dilution with 50 mmol/L ammonium bicarbonate, the samples were subjected to tryptic digestion at 37 °C for 18 h. The digested peptides were lyophilized and reconstituted in a freshly prepared solution composed of 0.1% (*v*/*v*) formic acid and 2% (*v*/*v*) acetonitrile in ultrapure water.

Peptides in the sample solution were separated *via* reverse-phase liquid chromatography using a Hypersil GOLD™ C18 column (100 mm × 2.1 mm, 3 μm, ThermoFisher Scientific, USA), which was eluted with a gradient of 2% to 95% (*v*/*v*) acetonitrile in 0.1% (*v*/*v*) formic acid at a flow rate of 0.4 mL/min for 10 min. Mass spectra were obtained with a full MS scan (200−2500 *m*/*z*, 70,000 resolution)[44], and an AGC target of 3×10^6, followed by data-dependent MS/MS analysis using a linear ion trap. Fragmentation of precursor ions was performed using higher-energy collisional dissociation (HCD) with a collision energy setting of 27 and an isolation window of *m*/*z* 4.0. The resulting MS/MS spectra were acquired at a resolution of 17,500, employing a maximum ion injection time of 50 ms and an automatic gain control (AGC) target value of 10^5 [44].

2.14. Cellular thermal shift assay

THP-1 cells were pre-incubated with either 40 μmol/L IAL or DMSO for 3 h, followed by lysis in PBS supplemented with protease inhibitors. Aliquots of 100 μL were exposed to a temperature gradient ranging from 37 to 65 °C for 3 min, rapidly frozen in liquid nitrogen, and then centrifuged at 12,000×*g* for 20 min at 4 °C. The resulting supernatants were denatured using loading buffer and subjected to Western blot analysis to evaluate TXNRD1 thermal stability.

2.15. Immunofluorescence assays

Cells or tissues were fixed with 4% paraformaldehyde (15 min), permeabilized with 0.1% Triton X-100 in PBS (30 min), and blocked with 1% BSA (2 h). Primary antibodies were incubated overnight at 4 °C, followed by species-matched fluorescent secondary antibodies (1 h, RT). Images were acquired using a Leica SP8 confocal microscope.

2.16. Statistical analysis

Statistical analysis was conducted using Prism 8 software (GraphPad, USA). All biological assays were repeated a minimum of two independent times, with triplicate samples included in each run. Representative experimental data are shown, expressed as mean ± standard deviation (SD). Differences between two groups were assessed using two-tailed Student's *t*-tests.

2.17. Ethics statement

All mice used in this study were obtained from Hangzhou Medical College (Hangzhou, China). Animal experiments were conducted in compliance with protocols approved by the Institutional Animal Care and Use Committee of Nanjing University of Chinese Medicine (No. SYXK-(Su) 2023-0076). The mice were maintained under standard housing conditions, including a temperature of 22−24 °C, a 12-h light/dark cycle, and relative humidity of 50 ± 10%, with *ad libitum* access to food and water.

3. Results

3.1. IAL reduces the viability of AML cells and triggers ROS generation

The cytotoxic effects of IAL were evaluated using the AML cell line THP-1. IAL significantly inhibited the viability of THP-1 cells after 24 h treatment, with a half-maximal inhibitory concentrations (IC_{50}) within 17.56 ± 3.14 μmol/L (Fig. 1A). Extensive studies have confirmed the critical role of intracellular ROS in the initiation, progression, and recurrence of tumors. Notably, ROS levels in AML cells markedly exceeded those in normal cells. Consequently, the 2′,7′-dichlorofluorescein diacetate (DCFH-DA) probe was employed to evaluate the impact of IAL treatment on ROS levels in AML cells. These findings indicated that IAL elicited ROS production in a dose-dependent manner. Furthermore, the addition of *N*-acetyl-L-cysteine (NAC), a principal ROS scavenger, completely reversed both the IAL-induced ROS production, underscoring the close association between the inhibitory effect of IAL and oxidative stress (Fig. 1B).

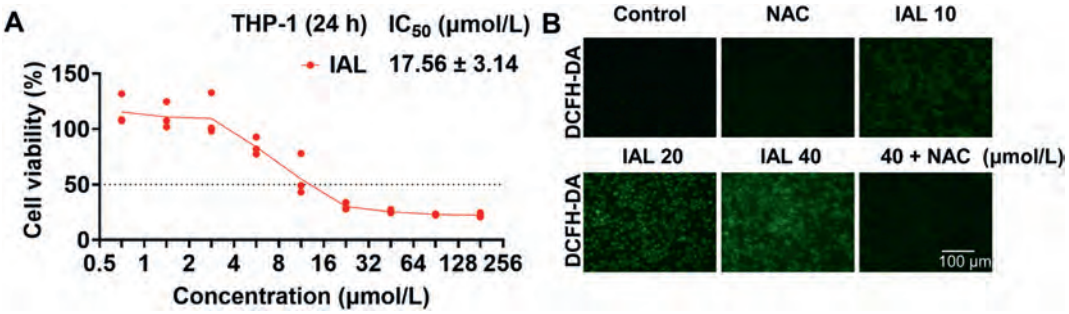

Figure 1 IAL inhibits the viability of AML cells and increases cellular ROS levels. (A) The IC_{50} values of IAL for THP-1 cells at 24 h. (B) Cellular ROS generation was detected by the DCFH-DA probes after the IAL treatment for 3 h. Cells were pretreated with 5 mmol/L NAC for 1 h. Scale bars: 100 μm. The data are present the mean ± SD, $n = 3$.

3.2. IAL induces pyroptosis in AML cells and enhances the efficacy of anti-PD-1 therapy

Considering the potential of a significant ROS surge to trigger cellular pyroptosis, the effect of IAL treatment on this process was explored in AML cells. Following treatment with IAL for 24 h, the AML cell line THP-1 displayed prominent pyroptosis markers, including extensive bubbling from the plasma membrane and significant cellular swelling (Fig. 2A). Morphological alterations in THP-1 cells following IAL treatment were subsequently analyzed using scanning electron microscopy (SEM) (Fig. 2B). Pyroptosis may be initiated *via* classical or nonclassical inflammasome pathways. Further investigations of the nonclassical inflammasome pathway demonstrated a marked elevation in the levels of GSDME-NT and cleaved-caspase-3 following IAL treatment in THP-1 cells (Fig. 2C).

Recent research indicates that pyroptosis can reshape the immune microenvironment in tumor cells by modulating the PD-1/PD-L1 immune checkpoint, potentially altering the efficacy of anti-PD-1 therapies. The activation of caspase-3 cleaves the poly ADP-ribose polymerase 1 (PARP-1), which increases the transcription of PD-L1, potentially enhancing responses in scenarios of limited efficacy of the anti-PD-1 antibody. To explore this mechanism, the effect of IAL treatment on the expression of PD-L1 was investigated (Fig. 2D). The results revealed that IAL upregulates the expression of PD-L1 in AML cells, potentially enhancing the efficacy of anti-PD-1 therapy. The effect of IAL treatment on the efficacy of anti-PD-1 therapy was further assessed by coculturing Phytohemagglutinin P (PHA-P) activated Jurkat T-cells with AML cells to evaluate the synergistic effects with anti-PD-1 treatment (Fig. 2E). The results suggest that IAL treatment may enhance t he therapeutic efficacy of anti-PD-1 treatment.

3.3. IAL directly targets the Sec^{498} of TXNRD1 in an irreversible manner

Given that IAL induces pyroptosis in AML cells and enhances the efficacy of anti-PD-1 therapy, we aimed to identify the direct or

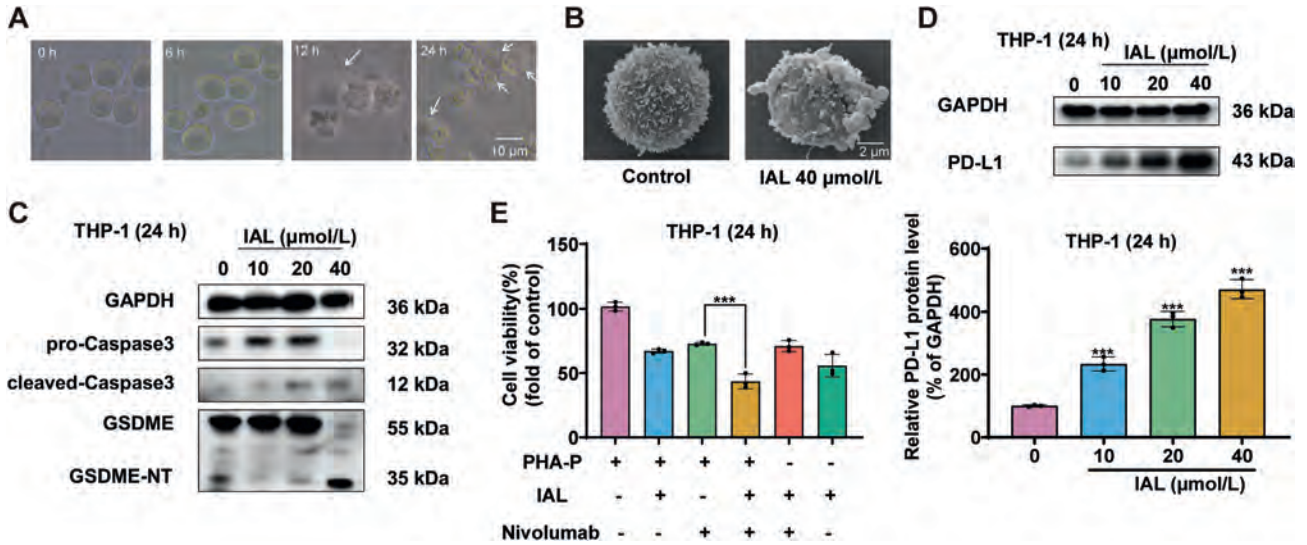

Figure 2 IAL induces pyroptosis of AML cells and enhances the efficacy of anti-PD-1 monoclonal antibody. (A) CLSM bright-field images of IAL (40 μmol/L) treated THP-1 cells collected at different time points. Scale bars: 10 μm. (B) Scanning electron microscopy (SEM) showed that AML cells treated with IAL (40 μmol/L) had pyroptosis compared with the control group, Scale bars: 2 μm. (C) Expression analysis of caspase-3 and GSDME in THP-1 cells after treating with IAL (0, 10, 20 and 40 μmol/L) for 24 h. (D) Expression analysis of PD-L1 in THP-1 cells using western blotting after the treatment with IAL (0, 10, 20 and 40 μmol/L) for 24 h and corresponding protein quantification. (E) After PHA-P activation, Jurkat-T cells were co-cultured with THP-1 cells upon IAL (10 μmol/L) treatment for 24 h. Error bars: SD, $n = 3$. Statistical significance of differences in mean values: $^{***}P < 0.001$.

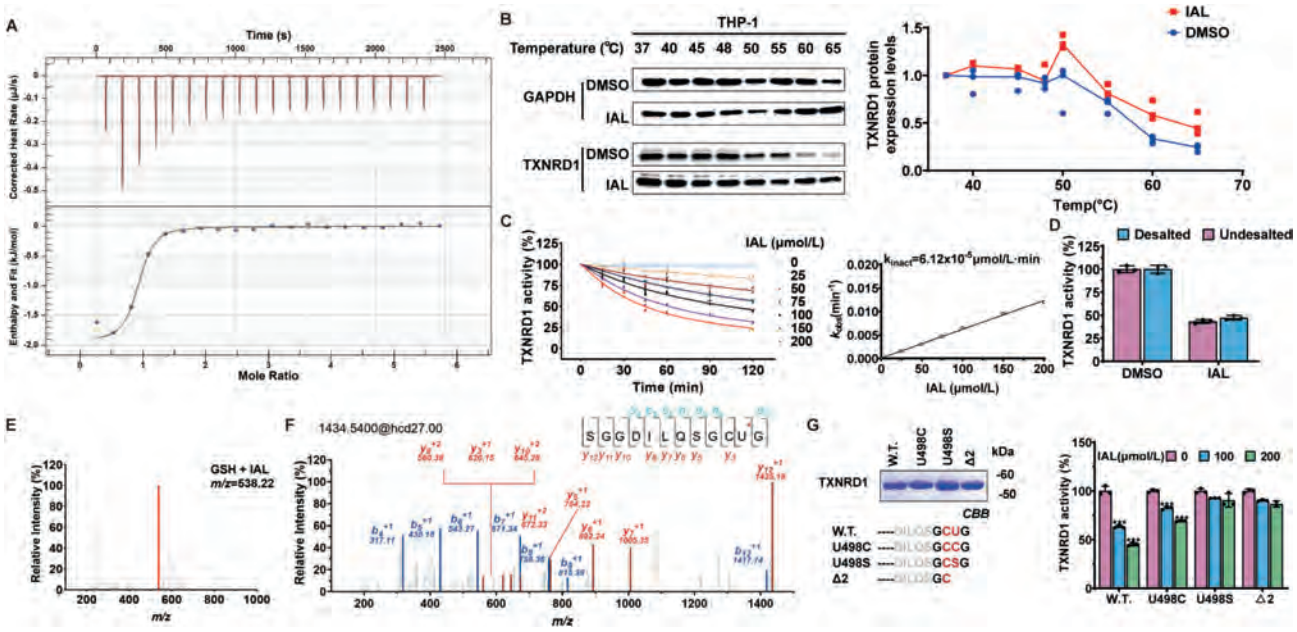

Figure 3 IAL directly targets the Sec^{498} residue of TXNRD1. (A) Isothermal titration calorimetry (ITC) analysis of IAL binding to TXNRD1. (B) THP-1 cells were incubated with IAL (40 μmol/L) or DMSO for 3 h. Subsequently, TXNRD1 protein expression was analyzed by Western blot under conditions where cell lysates were treated at varying temperatures. (C) Time−course inhibition of TXNRD1 by IAL 0.2 μmol/L pre-reduced TXNRD1 was incubated with IAL (0−200 μmol/L) for indicated time. The activity of the treated enzyme was assayed using DTNB reduction assay. (D) Irreversible inhibition of TXNRD1 by IAL 0.2 μmol/L pre-reduced TXNRD1 was incubated with 200 μmol/L IAL for 1 h, and then the enzyme was desalted using a desalting column. The DTNB reduction assay was used to determine the activity of TXNRD1. (E) Binding of GSH by IAL. (F) LC−MS/MS analysis of IAL-conjugated tryptic peptide of TXNRD1. "*m/z*" values covered the range from 100 to 1500. The majority target Sec abbreviated as U labeled with red asterisk. (G) Inhibitory effect of IAL on W.T. TXNRD1 and its mutant variants, Sec^{498} to cysteine (U498C), serine (U498S), and deletion (Δ2), respectively. Error bars: SD, $n = 3$. Statistical significance of differences in mean values: $^{***}P < 0.001$.

indirect targets of IAL. We previously established screening platform using a library of 127,695 compounds[42], and found that IAL is a potential small molecule binding to TXNRD1. We then used isothermal titration calorimetry (ITC) and determined that IAL binds to TXNRD1 with a K_d value of 8.392×10^{-8} mol/L, indicating strong binding affinity (Fig. 3A). This interaction between IAL and TXNRD1 was further confirmed *via* a cellular thermal shift assay (CETSA) (Fig. 3B). The impact of IAL on TXNRD1 activity was subsequently evaluated, and we found that IAL inhibits recombinant TXNRD1 activity in both dose- and time-dependent manner, with a K_{inact} constant of 6.12×10^{-5} L/μmol·min (Fig. 3C).

Next, we proposed that IAL may bind to TXNRD1 directly. To investigate the inhibition mechanism, free IAL molecules were removed from the incubation system using a G-25 desalting column and the residual TXNRD1 activity was measured using classic DTNB reducing activity assay. However, TXNRD1 activity was not recovered, suggesting that the binding of IAL to TXNRD1 is irreversible (Fig. 3D). Mass spectrometry (MS) analysis supported that IAL could form a stable adduct with GSH, indicating a thiol binding capacity of IAL (Fig. 3E). Furthermore, we aim to validate the binding of IAL to TXNRD1 using liquid chromatography−tandem MS (LC−MS/MS). We observed a precursor with a mass of 1434.54 Da, suggesting that one IAL molecule binding with the peptide at Sec^{498} (Fig. 3F).

The IAL binding to TXNRD1 was further investigated by site-directed mutagenesis through mutating the Sec^{498} residue of TXNRD1 to generate the reactive Cys^{498} residue (U498C), nonreactive Ser^{498} residue (U498S), and UGA-mediated deletion (Δ2 form). These TXNRD1 mutant variants were recombinantly expressed and purified, and then the enzymatic activities incubated with IAL were assessed and shown in Fig. 3G. Results showed that all three mutations mitigate the inhibitory effect of IAL on TXNRD1 activity.

Notably, the U498C mutant, in which cysteine shares similar properties with selenocysteine, retained substantial enzymatic activity and partially reversed the inhibitory effect of IAL. In contrast, both the U498S mutant and the U498-deletion (Δ2) mutant almost completely abolished the inhibitory effect of IAL on TXNRD1 enzymatic activity (Fig. 3G). These findings confirm that IAL directly targets the Sec^{498} residue of TXNRD1.

3.4. IAL selectively targets the Sec^{498} of TXNRD1 via Michael addition reaction

According to the established model for TXNRD1 inhibitors, the formation of a covalent bond between the Sec^{498} residue of TXNRD1 and the α,β-unsaturated carbonyl groups of the inhibitors is widely accepted[45]. To further explore the structure−activity relationship of IAL, the α,β-unsaturated double bond was chemically reduced to generate the reduced form of IAL (red. IAL) (Fig. 4A). The results demonstrated that red. IAL exerted minimal impact on the enzymatic activity of TXNRD1, underscoring the critical role of the α,β-unsaturated double bond of IAL as a functional group essential for the interaction with TXNRD1 (Fig. 4B). Additionally, the effects of reduced IAL on

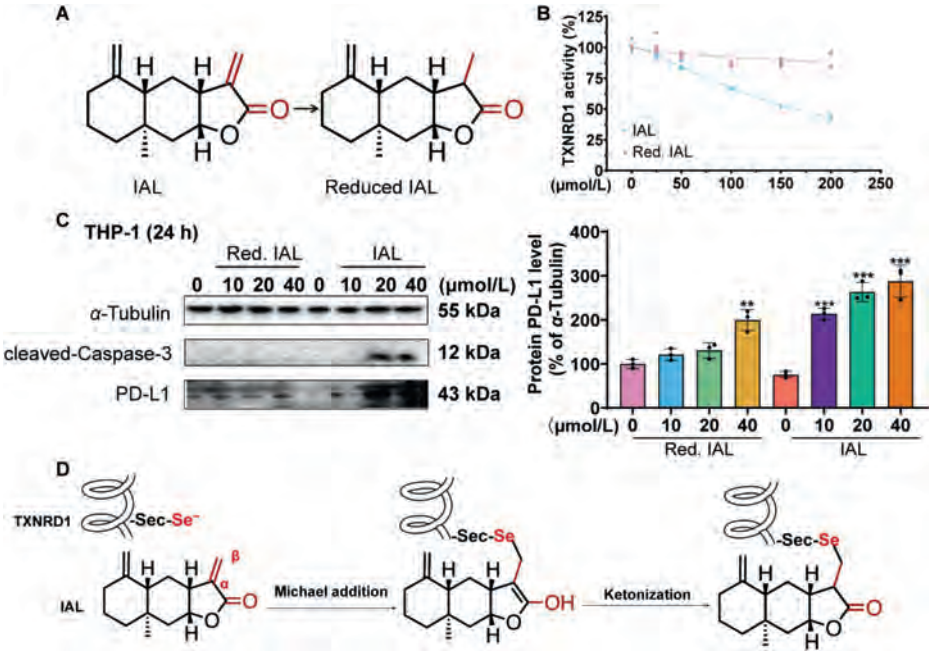

Figure 4 IAL targets the Sec^{498} of TXNRD1 *via* Michael addition reaction. (A) Chemical structures of IAL and reduced IAL. (B) The activity of TXNRD1 after treatment with IAL and reduced IAL (0−200 μmol/L). (C) Expression analysis of cleaved-caspase-3 and PD-L1 using Western blotting assay following the treatment of THP-1 cells with IAL and reduced IAL (0, 10, 20 and 40 μmol/L) for 24 h and corresponding protein quantification. (D) Schematic diagram illustrating the modification of IAL on TXNRD1. Error bars: SD, $n = 3$. Statistical significance of differences in mean values: $^{**}P < 0.01$, and $^{***}P < 0.001$.

the key pyroptosis-related proteins cleaved-caspase-3 were evaluated in AML cells. The red. IAL was found to induce negligible pyroptosis in AML cells (Fig. 4C). Furthermore, the red. IAL exerted little to no impact on the expression of PD-L1 in AML cells (Fig. 4C). Collectively, these findings confirm that IAL targets and inactivates TXNRD1 through a Michael addition reaction, where the selenol group of Sec^{498} binds the α,β-unsaturated carbonyl group of IAL (Fig. 4D). This molecular interaction likely underpins the observed impact of IAL treatment on pyroptosis and PD-L1 expression in AML cells, which aligns with the mechanistic framework proposed herein.

3.5. TXNRD1 is elevated in AML and negatively correlated with favorable prognosis

To explore the relationship between TXNRD1 and AML prognosis, the expression of endogenous TXNRD1 in primary AML cells was subsequently evaluated using immunofluorescence assays, which revealed predominant expression of the enzyme (Fig. 5A and Supporting Information Table S1, Fig. S1A). Kaplan−Meier survival analysis revealed that higher TXNRD1 expression correlated with poorer overall survival rate in AML patients, underscoring the pivotal role of TXNRD1 in the progression and maintenance of the disease (Fig. 5B). To ascertain whether TXNRD1 is a causative factor in AML or merely an incidental marker, the expression of TXNRD1 in AML cells was modulated using lentiviral systems to achieve significant knockdown, which was confirmed *via* Western blot analysis (Fig. 5C and Fig. S1B). Cell counting kit-8 (CCK-8) assays demonstrated that TXNRD1 knockdown markedly reduced the proliferation of THP-1 cells, suggesting that TXNRD1 can be exploited as a potential therapeutic target for inhibiting the growth of AML cells (Fig. 5D). Additionally, immunofluorescence assays indicated a decrease in Ki-67 expression following TXNRD1 knockdown, further supporting the potential of targeting TXNRD1 to impair AML cell viability (Fig. 5E).

3.6. TXNRD1 inhibitor auranofin induces oxidative stress and pyroptosis in AML

Given our previous findings that targeting TXNRD1 can induce pyroptosis in AML cells, we selected the FDA-approved TXNRD1 inhibitor auranofin (AF), its effect on the growth of AML cells was subsequently evaluated. AF treatment effectively reduced the viability of the AML cell lines THP-1 and primary AML cells, this effect was reversed upon treatment with NAC (Fig. 6A and B). The DCFH-DA probe was employed for elucidating the mechanism of ROS induction by AF in AML cells (Fig. 6C). We then focus on hydrogen peroxide (H_2O_2), a crucial molecule in redox signaling. A detailed assessment of H_2O_2 generation within various cellular organelles was conducted in THP-1 cells after 12 h AF treatment by utilizing specifically-designed HyPer sensor proteins targeted to distinct organelles (cytosol, nucleus, peroxisome, mitochondria, and ER). Notably, pretreatment with NAC completely reversing these effects, underscoring the role of TXNRD1 inhibition in inducing oxidative stress (Fig. 6D and E).

The impact of targeting TXNRD1 on pyroptosis in AML cells was subsequently evaluated. We examined the effect of AF on pyroptosis in AML cells and both SEM and Western Blot results showed that AF increased pyroptosis in AML cells. In this experiment, AF treatment resulted in the induction of pyroptosis *via* the nonclassical pathway in both THP-1 cells and primary AML cells (Fig. 6F−H). These findings highlight the multifaceted role of TXNRD1 as a therapeutic target in AML.

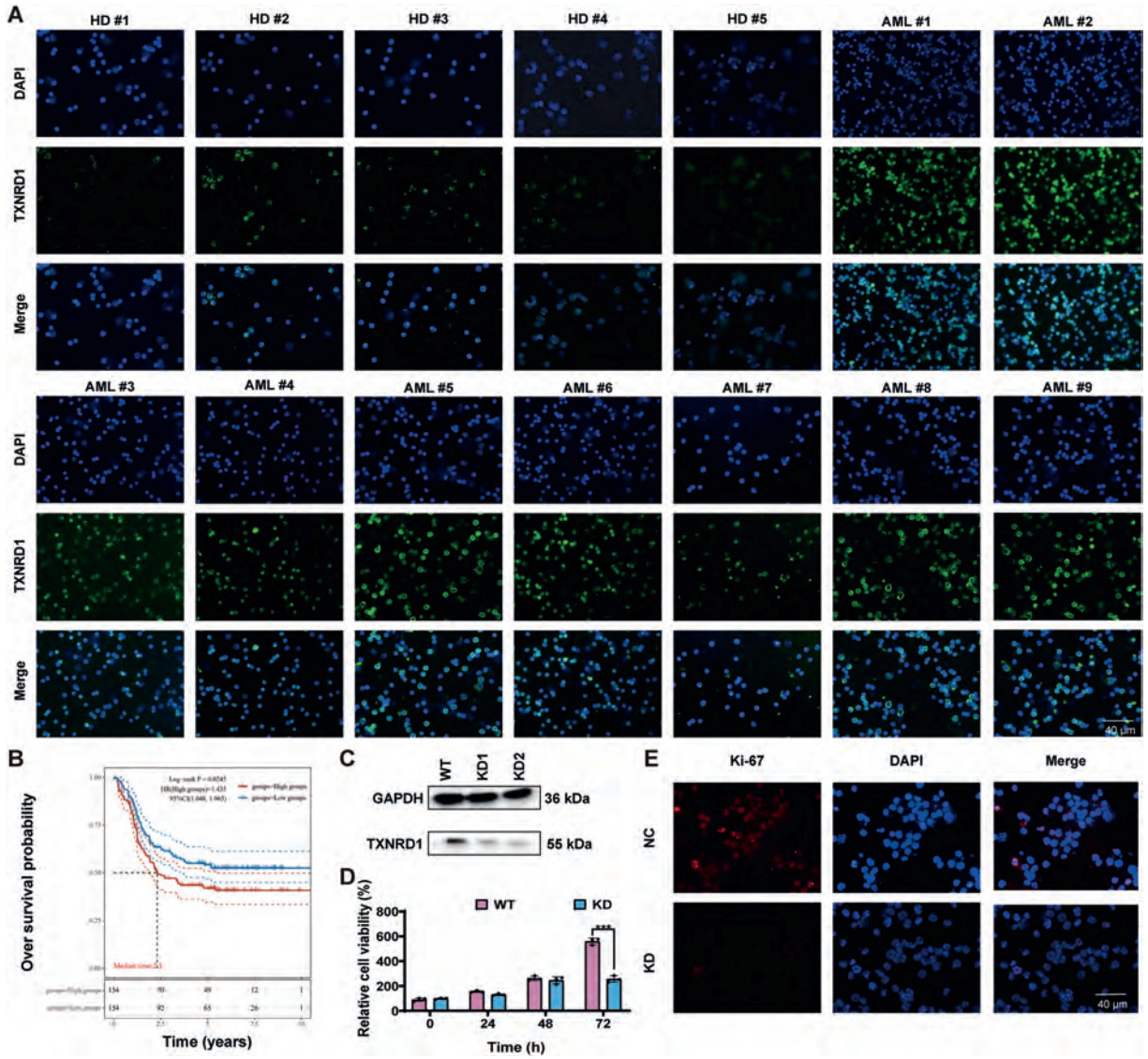

Figure 5 TXNRD1 is elevated in AML and negatively correlated with favorable prognosis. (A) Immunofluorescence analysis of TXNRD1 in healthy donors (HDs) and AML patients. Scale bars: 40 μm. (B) Kaplan−Meier survival analysis was used to detect the relationship between TXNRD1 high expression and overall survival rate of AML patients. (C) Western blot was used to detect the expression of TXNRD1 in THP-1, KD1 and KD2 cell lines. (D) CCK-8 assay for evaluating cell proliferation and viability in wild-type (WT) and TXNRD1 knockdown (TXNRD1-KD1) cell lines. (E) Immunofluorescence was used to analyze the effect of normal cell lines (NC) and knockdown cell lines (KD1) on cell proliferation. Scale bars: 40 μm. Error bars: SD, $n = 3$. Statistical significance of differences in mean values: $^{***}P < 0.001$.

3.7. TXNRD1 inhibitor induces pyroptosis in AML cells via PPARγ activation

Previous studies have established that the anti-AML properties of IAL are mediated *via* the direct inhibition of TXNRD1 activity. To elucidate the mechanism by which TXNRD1 inhibition promotes pyroptosis in AML cells, transcriptome analysis was performed following treatment with the TXNRD1 inhibitor AF. KEGG pathway analysis identified the top ten most significantly altered pathways. TXNRD1 serves as the exclusive enzyme that catalyzes disulfide bond reduction in thioredoxin substrates, highlighting its critical role in redox homeostasis—a function parallel to PPAR in cellular regulation. Furthermore, PPAR, a ligand-activated transcription factor in the nuclear hormone receptor superfamily, forms heterodimers with RXRα and has been shown to modulate immune and inflammatory responses in AML cells. Based on these findings, we selected PPAR for further investigation (Fig. 7A). The impact of AF on the protein levels of three PPAR isoforms including PPARα, PPARβ, and PPARγ, was subsequently investigated. As shown in Fig. 7B, AF was found to significantly elevate the expression of PPARγ, while exerting minimal effects on the other two isoforms (Fig. 7B). The AF-induced increase in PPARγ expression was reversed by the PPARγ-specific inhibitor GW9662. This result underscores PPARγ as a critical downstream mediator of TXNRD1 inhibition in AML (Fig. 7C).

The nuclear translocation of PPARγ following AF treatment is a critical step for its activity. Thus, the distribution of PPARγ in THP-1 cells was subsequently assessed. The data depicted in Fig. 7D demonstrate that AF treatment facilitated the nuclear accumulation of PPARγ and concomitantly decreased its

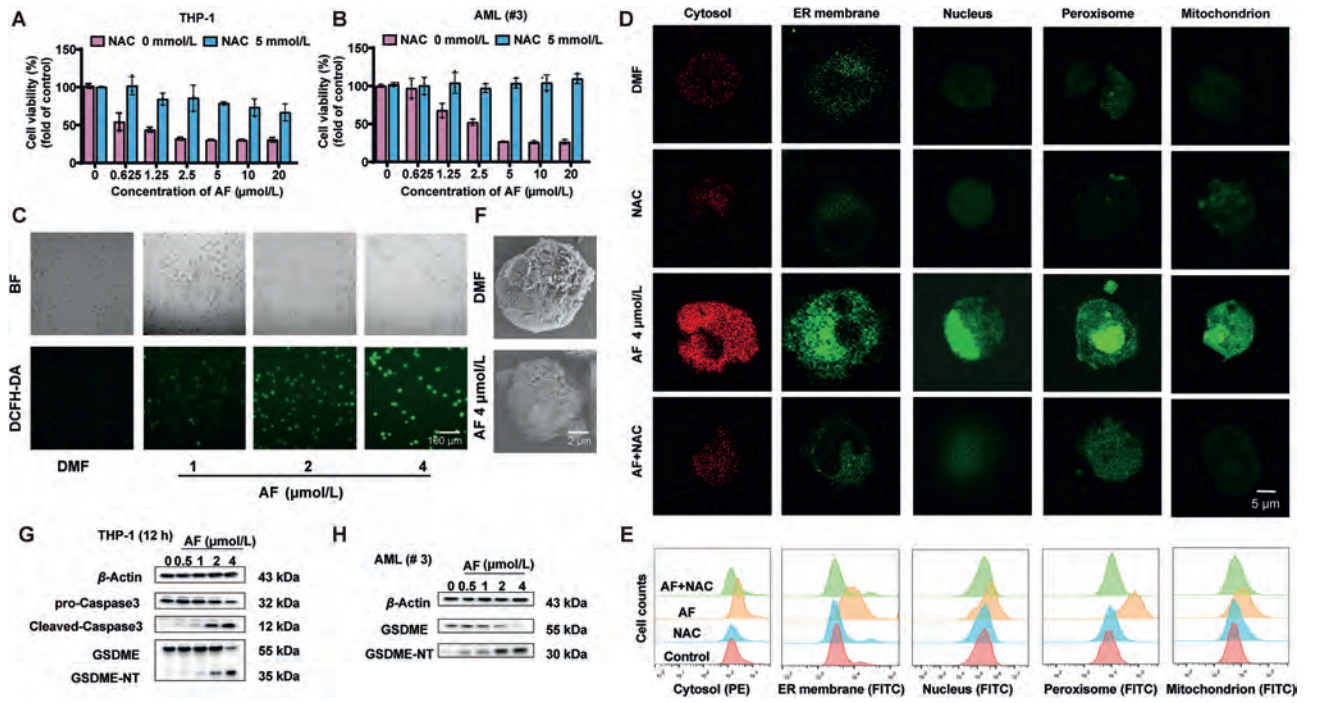

Figure 6 AF induces oxidative stress and pyroptosis in AML cell line THP-1 and AML patients. (A, B) The cell viability of AF at concentrations ranging from 0 to 20 μmol/L at 72 h in THP-1 and primary AML cells (#3), countervailing effect of the NAC by the CCK-8 assay. NAC pretreatment was performed at 5 mmol/L for 1 h. (C) Cellular ROS generation was detected by the DCFH-DA probes after the AF treatment for 3 h. (D) Localizations of HyPer response in THP-1 cells following exposure to AF (4 μmol/L) for 12 h. NAC (5 mmol/L) pretreatment was performed for 1 h. HyPer response in different cell compartments (cytosol, ER membrane, nucleus, peroxisome, and mitochondrion) was visualized. Scale bars: 5 μm. (E) Flow cytometry was used to analyze HyPer response in the organelles (cytosol, ER membrane, nucleus, peroxisome, and mitochondrion) induced by AF. (F) Scanning electron microscopy (SEM) showed that AML cells treated with AF (4 μmol/L) had pyroptosis compared with the control group. Scale bars: 2 μm. (G) Expression analysis of caspase-3 and GSDME using Western blot following the treatment of THP-1 cells with AF (0, 0.5, 1, 2 and 4 μmol/L) for 12 h. (H) The expression of GSDME in primary patient cells (AML #3) after AF treatment was detected by Western blot. Error bars: SD, $n = 3$.

cytoplasmic localization. Caspase-3, a key downstream effector of PPARγ, is activated *via* this pathway. TXNRD1 inhibition results in PPARγ activation, subsequently initiating the caspase-3-dependent noncanonical pathway of pyroptosis. This comprehensive analysis confirms the role of the PPARγ pathway in mediating the pyroptotic response to TXNRD1 inhibition in AML.

3.8. IAL exhibits antileukemic effects in a NOD/SCID mouse model bearing patient-derived AML cells

To evaluate the anti-AML effects of IAL *in vivo*, primary AML samples were employed for the inoculation of NOD/SCID mice, with doxorubicin (1.25 mg/kg) and AF (5 mg/kg) employed as the conventional and target-specific positive control, respectively. The mice exhibited AML symptoms two weeks after inoculation. Three randomly-selected mice from each group were then euthanized, revealing a pronounced reduction in splenomegaly in the IAL-treated group (Fig. 8A). Monitoring of the weights of the body revealed minimal effects of IAL on the overall body weight (Fig. 8B). Additionally, IAL treatment led to a reduction in the number of huCD45$^+$ cells in the bone marrow, indicative of a therapeutic impact on AML (Fig. 8C). Kaplan−Meier survival analysis revealed that IAL treatment significantly extended the survival of the AML-bearing mice (Fig. 8D and Supporting Information Table S2). This comprehensive assessment underscores the potential of employing IAL as a therapeutic option for AML, given its favorable safety and efficacy profiles in animal models.

3.9. IAL enhances the efficacy of anti-PD-1 therapy and reshapes the immune microenvironment in vivo

The therapeutic efficacy of combined IAL and anti-PD-1 treatment and its impact on the immune microenvironment were evaluated in a murine model of AML. C57BL/6 mice were intravenously inoculated with murine myeloid leukemia cells C1498 cells expressing luciferase (Fig. 9A). Doxorubicin (1.25 mg/kg), AF (5 mg/kg), and anti-PD-1 antibodies served as controls. The intensity of bioluminescence, used to assess treatment efficacy, was notably lowest in the group that received the combination of IAL and anti-PD-1, suggesting the most effective therapeutic outcome in this group. This observation was further corroborated by significant therapeutic activity in the group treated with the combination of AF and anti-PD-1 antibodies. Furthermore, the combinations alleviated splenomegaly (Fig. 9B).

Subsequent analysis focused on key immune markers in the treated groups. The group that received combined treatment with IAL and anti-PD-1 antibodies exhibited enhanced immune activation compared to that in the untreated group, surpassing the effects seen with the AF and anti-PD-1 combination. While IAL monotherapy induced immune activation, it was less pronounced than that observed with the combination treatments. Notably, there

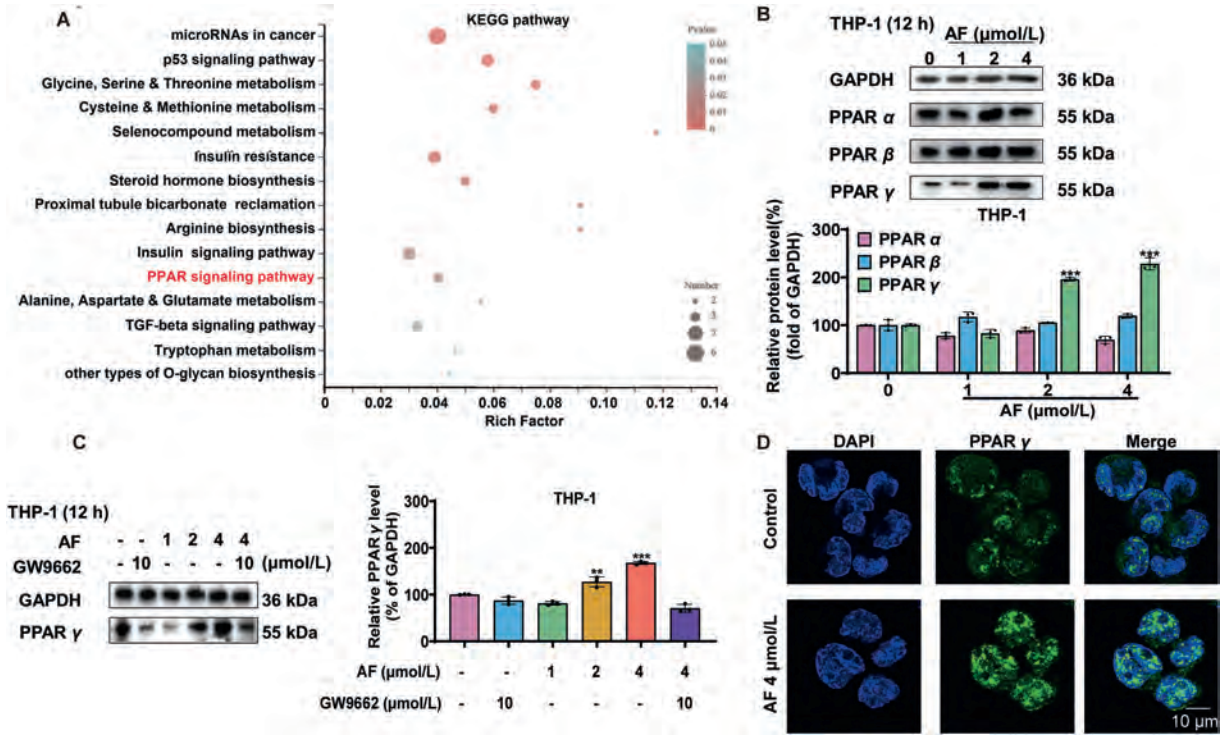

Figure 7 AF induces pyroptosis in AML cells *via* PPARγ activation. (A) Kyoto Encyclopedia of Genes and Genomes (KEGG) enrichment analysis of the differentially expressed genes after AF treatment. (B) Expression analysis of PPARα, PPARβ, PPARγ using Western blot following the treatment of THP-1 cells with AF (0, 1, 2 and 4 μmol/L) for 12 h. (C) Expression analysis of PPARγ in THP-1 cells using Western blot following AF (0, 1, 2 and 4 μmol/L) treatment in the absence or presence of 10 μmol/L GW9662. (D) Immunofluorescence analysis was used to detect the expression of PPARγ after AF (4 μmol/L) treatment. Scale bars: 10 μm. Error bars: SD, $n = 3$. Statistical significance of differences in mean values: $^{**}P < 0.01$ and $^{***}P < 0.001$.

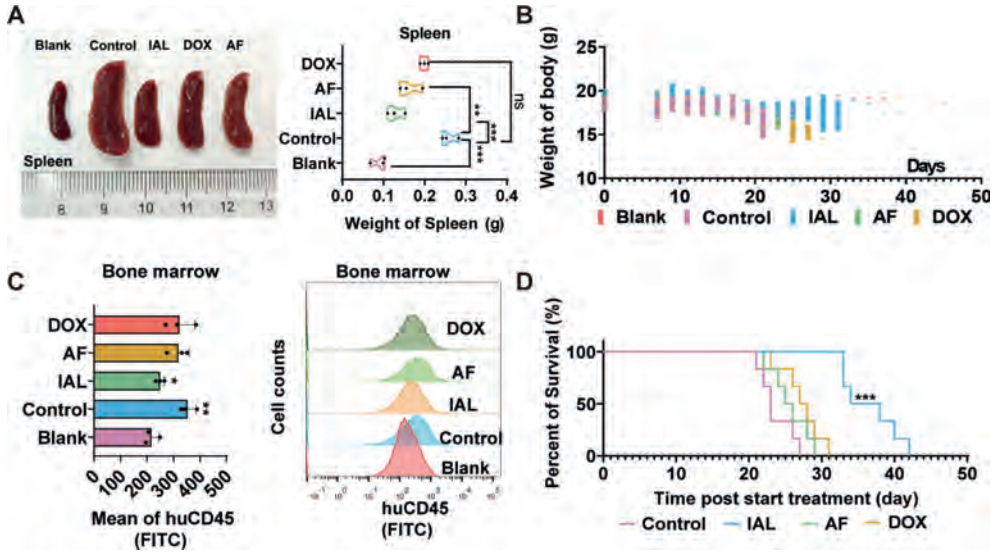

Figure 8 *In vivo* antitumor activity of IAL by PDX. (A) Effects of IAL (30 mg/kg), AF (5 mg/kg), and DOX (1.25 mg/kg) on the weight of the spleen in NOD/SCID mice bearing primary AML cells. (B) Body weight changes in NOD-SCID mice separately treated with IAL (30 mg/kg), AF (5 mg/kg), and DOX (1.25 mg/kg). (C) The expression of huCD45 (FITC) in bone marrow cells of each group was analyzed by using flow cytometry. (D) Kaplan−Meier survival curves of AML cells bearing NOD/SCID and treated with IAL, AF, and DOX, respectively. Error bars: SD, $n = 3$. Statistical significance of differences in mean values: $^{*}P < 0.05$, $^{**}P < 0.01$, and $^{***}P < 0.001$.

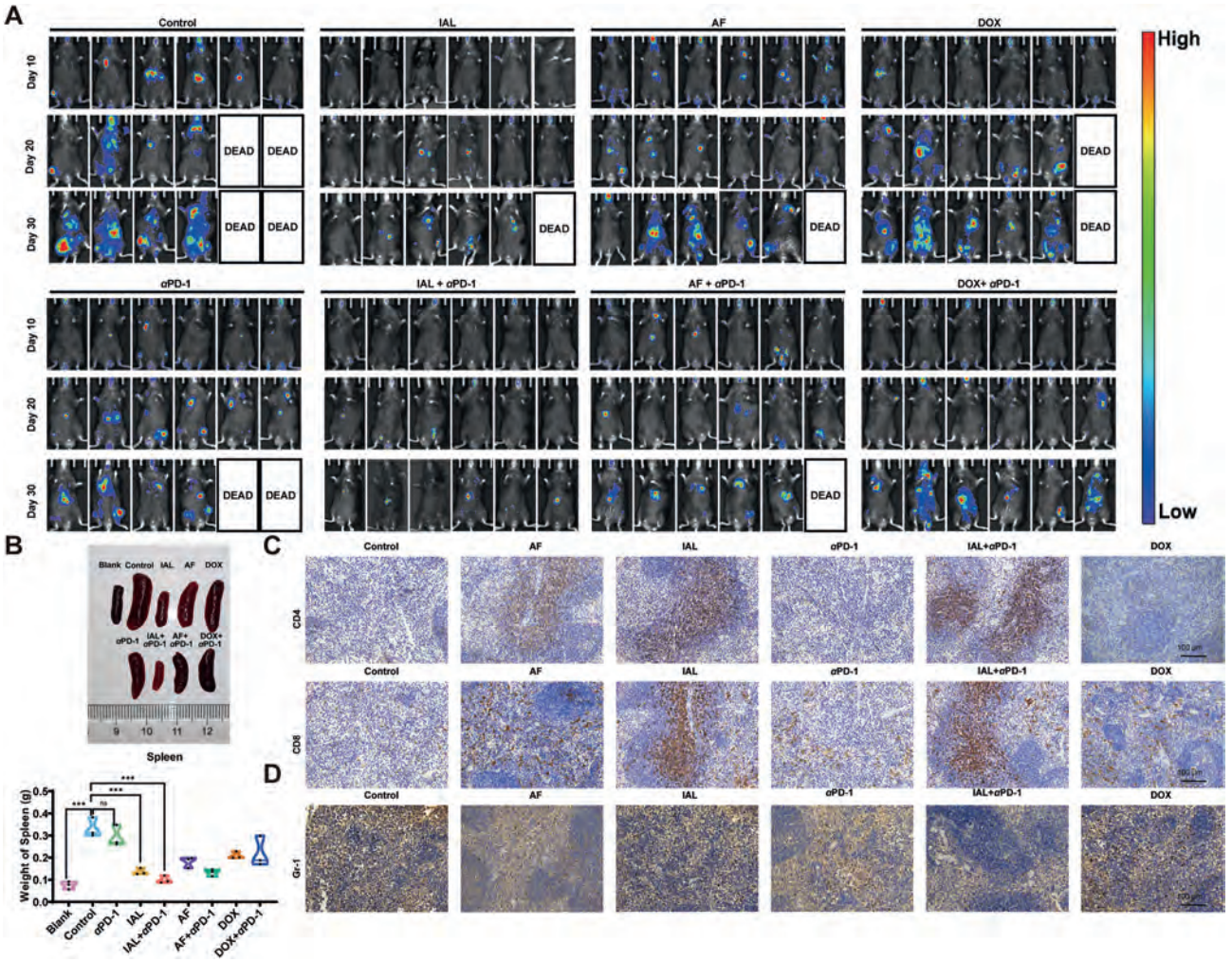

Figure 9 Antitumor activity of IAL *in vivo* in C57BL/6 mice. (A) *In vivo* antitumor activity of IAL and tumor imaging in C57BL/6 mice. (B) Changes in spleen size of tumor-bearing mice in different treatment groups. (C) Immunohistochemistry (IHC) was used to detect the changes of CD4 and CD8 in the spleen of C57BL/6 mice bearing luc-C1498 cells in different treatment groups. Scale bars:100 μm. (D) Representative micrographs of IHC staining of Gr-1 in the spleen of C57BL/6 mice bearing luc-C1498 cells. Scale bars: 100 μm. Error bars: SD, $n = 3$. Statistical significance of differences in mean values: $^{***}P < 0.001$.

was an increase in the numbers of $CD4^+$ and $CD8^+$ T cells, after the treatment of IAL (Fig. 9C). Conversely, the numbers of immunosuppressive cells such as MDSCs were decreased (Fig. 9D). These findings underscore the potential of IAL treatment and the consequent TXNRD1 inhibition for favorably modifying the immune microenvironment in AML, fostering an immunostimulatory profile that augments therapeutic efficacy. This comprehensive evaluation highlights the potential of IAL in combinantion treatment with immune checkpoint inhibitors to enhance antitumor responses in AML.

To investigate the anti-AML mechanism of IAL *in vivo*, we established a C57BL/6 mouse model with subcutaneous C1498 cell inoculation and evaluated tumor size (Fig. 10A). Results showed that both AF and IAL reduced tumor weight and volume (Fig. 10B and C), consistent with previous findings. Western blot analysis revealed that AF and IAL effectively decreased TXNRD1 levels, activating PPARγ. This led to upregulation of caspase-3 transcription, enhanced cleavage of GSDME, and ultimately induced pyroptosis (Fig. 10D and E).

4. Discussions

TXNRD plays a key role in combating oxidative stress in AML[46]. The inhibition of TXNRD1 regulates the activity of glyceraldehyde-3-phosphate dehydrogenase, disrupting glycolysis and enhancing the flux through the pentose phosphate pathway (PPP)[31]. TXNRD1 inhibitors such as beta-lapachone have shown efficacy in inhibiting the proliferation of AML cells[47]. There is increasing evidence that TXNRD1-mediated redox balance directly impairs anti-tumor immunity. Elevated TXNRD1 activity in AML cells can lead to an imbalance of intracellular ROS. This imbalance disrupts the immune microenvironment *in vivo* by impairing the cross-presentation of antigens between DCs and T cells and enhancing the activity of immune-suppressive MDSCs and Tregs[48]. However, the feasibility of targeting TXNRD1 in AML using clinical specimens remains to be established. The current study uses clinical sample analyses to demonstrate that TXNRD1 is overexpressed in AML cells compared to normal cells. This overexpression correlates with poorer survival outcomes in patients with AML, supporting the

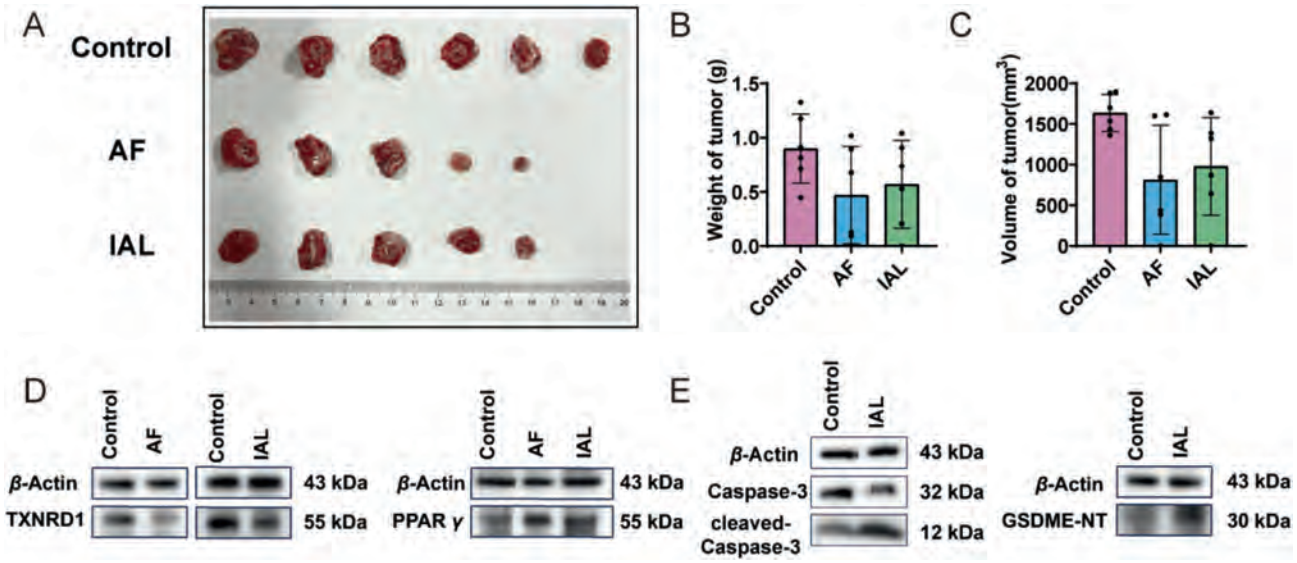

Figure 10 CDX model of AML *in vivo* in C57BL/6 mice. (A) Changes in tumor size after AF and IAL treatment. (B) Tumor weight after AF and IAL treatment. (C) Changes in tumor volume after AF and IAL treatment. (D) Expression of TXNRD1 and PPARγ in tumors after AF and IAL treatment. (E) Changes in caspase-3 and GSDME-NT levels after IAL treatment.

rationale for exploiting TXNRD1 as a therapeutic target in AML. Oxidative stress is known to activate a range of transcription factors that are critical for the pathogenesis of AML, including but not limited to NF-κB, nuclear respiratory factor 1 (Nrf1), p53, PPARγ, STAT3, AKT, and forkhead box protein (FOXO)[49]. The associations between TXNRD1 and these transcription factors remain unclarified. Transcriptome sequencing identified a direct association between TXNRD1 and PPARγ. This novel interaction pathway in AML suggests a previously unrecognized mechanism linking redox regulation to transcriptional control of pyroptosis. Additionally, the inhibition of the nuclear translocation of PPARγ allows the regulation of caspase 3 transcription; this is relevant given that caspase-3 cleaves GSDME, an executor of the nonclassical pathway of pyroptosis, highlighting the association between TXNRD1 and pyroptosis.

Pyroptosis is a form of inflammatory cell death, and its induction in tumor cells is likely to modify the tumor microenvironment. One of the primary reasons for the poor efficacy of the anti-PD-1 monoclonal antibody therapy in AML is the immunosuppressive tumor microenvironment, characterized by a lack of neoantigen repertoire and an immune-excluded or immune-desert phenotype with deficient or inactive tumor-infiltrating lymphocytes[50−52]. The current study finds that inducing pyroptosis in AML cells enhances their response to PD-1 blockade. This effect is due to the activation of caspase-3, which induces the cleavage of PARP-1, leading to an increase in the expression of PD-L1 and heightened sensitivity to anti-PD-1 monoclonal antibodies[53,54]. Additionally, the release of IL-1, IL-18, and high mobility group box 1 (HMGB1) from tumor cells undergoing pyroptosis triggers immunogenic cell death and activates immune cells such as DCs, macrophages, and NK cells[55]. This process promotes the infiltration of cytotoxic T-lymphocytes. Employing this "one−two punch" strategy may be an effective approach for enhancing antitumor effects by converting "cold" tumors into "hot" tumors[56,57].

Currently, the use of natural compounds and drug repurposing are important strategies for enhancing the efficiency of drug development[58]. The formation of covalent bonds with Sec^{498} of TXNRD1 is major mechanism of TXNRD1 inhibition[59,60]. Several low-molecule-weight inhibitors, such as piperlongumine and shikonin[59,61], have been identified to target Sec^{498}, leading to effective TXNRD1 inhibition. Additionally, modifications at N-terminal Cys residues (Cys^{58} and Cys^{62}) may impact enzymatic activity, while Cys^{189} has also been suggested as a potential interaction site with gold complexes[63]. Interestingly, Sanguinarine[62] and chaetocin[64] are universally recognized to form two hydrogen bonds with the residue Glu^{477} of TXNRD1 *via* the phenanthridinium group at their electrophilic center, effectively inactivating TXNRD1. A previous study from our group screened 127,695 compounds and identified 10 potential inhibitors of TXNRD1, including IAL. In this study, we revealed that IAL induces pyroptosis in AML cells and enhances the efficacy of anti-PD-1 therapy utilizing a monoclonal antibody. The binding of IAL to TXNRD1 was initially confirmed using CETSA, and enzyme assays revealed that IAL significantly inhibits TXNRD1 activity. Further LC−MS/MS analysis confirmed the direct binding of IAL with Sec^{498} of TXNRD1 through a Michael addition reaction. Additionlly, the GSH depletion activity of IAL may contribute to the cytotoxicity of IAL in AML.

The *in vivo* antitumor effects of IAL were validated using a patient-derived xenograft model that utilized primary AML cells. The results showed that IAL treatment significantly inhibited the infiltration of AML cells into the bone marrow of inoculated mice. To evaluate the impact of IAL treatment on the immune microenvironment, a murine C1498 AML model was constructed in C57 mice. The results demonstrated that IAL not only reduced the AML burden and ameliorated splenomegaly in inoculated mice but also enhanced the efficacy of anti-PD-1 monoclonal antibody therapy. Furthermore, an analysis of the immune microenvironment revealed that IAL increased the numbers of T-cells while reducing those of MDSCs, providing a strategy for improving the immunosuppressive microenvironment in AML.

While our study provides mechanistic insights into TXNRD1 inhibition in AML, several limitations should be acknowledged.

First, the sample size of the clinical samples analyzed here was limited, and given the epigenetic heterogeneity of AML, future multicenter studies with larger cohorts are needed to validate the prognostic significance of TXNRD1 in different AML subtypes. Second, while our *in vivo* experiments in NOD/SCID mice demonstrated the anti-leukemic effects of IAL, these models may not fully recapitulate the complexity of the human AML immune microenvironment. Third, although we identified PPARγ as a downstream mediator of TXNRD1 inhibition, the precise molecular mechanisms linking TXNRD1 to PPARγ activation remain incompletely defined.

5. Conclusions

In summary, the current study employed clinical samples to demonstrate the feasibility of targeting TXNRD1 as a therapeutic approach for AML. Further, the transcription factor PPARγ was identified to play a direct role in AML and regulate caspase-3 expression to activate GSDME-dependent pyroptosis, thereby enhancing the efficacy of anti-PD-1 monoclonal antibody therapy. Additionally, this study established IAL as the original molecular template for TXNRD1 inhibition. Further research using IAL with chemically synthesized structural modifications may reveal more promising candidates for TXNRD1 inhibition with greater bioactivity and fewer off-target effects that are suitable for clinical translation.

Acknowledgements

This work was supported by the National Natural Science Foundation of China (82574638 and 82204443), the high level key discipline construction project of the National Administration of Traditional Chinese Medicine-Resource Chemistry of Chinese Medicinal Materials (No. zyyzdxk-2023083, China) and Yunnan Provincial Science and Technology Talent and Platform Program (No. 202405AF140031, China). The graphical abstract was created with BioRender.com and published with permission.

Author contributions

Xiaoxuan Yu designed and performed research, analyzed data, and wrote the paper; Yanyu Zhou and Shibo Sun analyzed data and maintained research data. Lu Tang and Wan Zhang provided the preparation and creation of figures. Wukun Liu, Jianqiang Xu and Xiaoxuan Yu conceptualized and financial supported for the project, and directed the experimental design and data analysis.

Conflicts of interest

The authors declare that they have no known competing financial interests or personal relationships that could have appeared to influence the work reported in this paper.

Appendix A. Supporting information

Supporting information to this article can be found online at https://doi.org/10.1016/j.apsb.2025.12.040.

References

1. Bray F, Laversanne M, Sung H, Ferlay J, Siegel RL, Soerjomataram I, et al. Global cancer statistics 2022: GLOBOCAN estimates of incidence and mortality worldwide for 36 cancers in 185 countries. *CA Cancer J Clin* 2024;**74**:229−63.
2. Alves da Silva PH, Xing S, Kotini AG, Papapetrou EP, Song X, Wucherpfennig KW, et al. MICA/B antibody induces macrophage-mediated immunity against acute myeloid leukemia. *Blood* 2022; **139**:205−16.
3. Yates JW, Wallace Jr HJ, Ellison RR, Holland JF. Cytosine arabinoside (NSC-63878) and daunorubicin (NSC-83142) therapy in acute nonlymphocytic leukemia. *Cancer Chemother Rep* 1973;**57**:485−8.
4. Larson RA, Mandrekar SJ, Huebner LJ, Sanford BL, Laumann K, Geyer S, et al. Midostaurin reduces relapse in FLT3-mutant acute myeloid leukemia: the Alliance CALGB 10603/RATIFY trial. *Leukemia* 2021;**35**:2539−51.
5. Bruzzese A, Labanca C, Martino EA, Mendicino F, Lucia E, Olivito V, et al. Ivosidenib in acute myeloid leukemia. *Expet Opin Pharmacother* 2023;**24**:2093−100.
6. Hu M, Li W, Zhang Y, Liang C, Tan J, Wang Y. Venetoclax in adult acute myeloid leukemia. *Biomed Pharmacother* 2023;**168**: 115820.
7. Shi Z, Bai H, Wu J, Miao X, Gao J, Xu X, et al. Acceptor engineering produces ultrafast nonradiative decay in NIR-II Aza-BODIPY nanoparticles for efficient osteosarcoma photothermal therapy via concurrent apoptosis and pyroptosis. *Research* 2023;**6**:169.
8. Desai A, Gainor J, Hegde A, Schram A, Curigliano G, Pal S, et al. COVID-19 vaccine guidance for patients with cancer participating in oncology clinical trials. *Nat Rev Clin Oncol* 2021;**18**:313−9.
9. Wang M, Zhang C, Tian T, Zhang T, Wang R, Han F, et al. Increased regulatory T cells in peripheral blood of acute myeloid leukemia patients rely on tumor necrosis factor (TNF)-α−TNF receptor-2 pathway. *Front Immunol* 2018;**9**:1274.
10. Vago L, Gojo I. Immune escape and immunotherapy of acute myeloid leukemia. *J Clin Investig* 2020;**130**:1552−64.
11. Binder S, Luciano M, Horejs-Hoeck J. The cytokine network in acute myeloid leukemia (AML): a focus on pro- and anti-inflammatory mediators. *Cytokine Growth Factor Rev* 2018;**43**:8−15.
12. Huang G, Shen H, Xu K, Shen Y, Jiale J, Chu G, et al. Single-cell microgel encapsulation improves the therapeutic efficacy of mesenchymal stem cells in treating intervertebral disc degeneration via inhibiting pyroptosis. *Research* 2024;**7**:311.
13. Ozkazanc D, Yoyen-Ermis D, Tavukcuoglu E, Buyukasik Y, Esendagli G. Functional exhaustion of $CD4^+$ T cells induced by co-stimulatory signals from myeloid leukaemia cells. *Immunology* 2016; **149**:460−71.
14. Liu G, Zhang Q, Yang J, Li X, Xian L, Li W, et al. Increased TIGIT expressing NK cells with dysfunctional phenotype in AML patients correlated with poor prognosis. *Cancer Immunol Immunother* 2021; **71**:277−87.
15. Tettamanti S, Pievani A, Biondi A, Dotti G, Serafini M. Catch me if you can: how AML and its niche escape immunotherapy. *Leukemia* 2021;**36**:13−22.
16. Alves da Silva PH, Xing S, Kotini AG, Papapetrou EP, Song X, Wucherpfennig KW, et al. MICA/B antibody induces macrophage-mediated immunity against acute myeloid leukemia. *Blood* 2022; **139**:205−16.
17. Daver N, Kontoyiannis DP. Checkpoint inhibitors and aspergillosis in AML: the double hit hypothesis. *Lancet Oncol* 2017;**18**:1571−3.
18. Daver N, Garcia-Manero G, Basu S, Boddu PC, Alfayez M, Cortes JE. Efficacy, safety, and biomarkers of response to azacitidine and nivolumab in relapsed/refractory acute myeloid leukemia: a nonrandomized, open-label, phase II study. *Cancer Discov* 2019;**9**: 370−83.
19. Yang X, Ma L, Zhang X, Huang L, Wei J. Targeting PD-1/PD-L1 pathway in myelodysplastic syndromes and acute myeloid leukemia. *Exp Hematol Oncol* 2022;**11**:11.

20. Yu X, Cai L, Yao J, Li C, Wang X. Agonists and inhibitors of the cGAS−STING pathway. *Molecules* 2024;**29**:3121.
21. Zeidan AM, Boss I, Beach CL, Copeland WB, Thompson E, Fox BA, et al. A randomized phase 2 trial of azacitidine with or without durvalumab as first-line therapy for older patients with AML. *Blood Adv* 2022;**6**:2219−29.
22. Lecciso M, Ocadlikova D, Sangaletti S, Trabanelli S, De Marchi E, Orioli E, et al. ATP release from chemotherapy-treated dying leukemia cells elicits an immune suppressive effect by increasing regulatory t cells and tolerogenic dendritic cells. *Front Immunol* 2017;**8**:1918.
23. Zhang Y, Zhao W, Wu L, Ai T, He J, Chen Z, et al. Inhibition of CCT5-mediated asparagine biosynthesis and anti-PD-L1 produce synergistic antitumor effects in colorectal cancer. *Acta Pharm Sin B* 2025;**15**:2480−97.
24. Junn E, Han SH, Im JY, Yang Y, Cho EW, Um HD, et al. Vitamin D3 up-regulated protein 1 mediates oxidative stress *via* suppressing the thioredoxin function. *J Immunol* 2000;**164**:6287−95.
25. An X, Yu W, Liu J, Tang D, Yang L, Chen X. Oxidative cell death in cancer: mechanisms and therapeutic opportunities. *Cell Death Dis* 2024;**15**:556.
26. Man SM, Karki R, Kanneganti TD. Molecular mechanisms and functions of pyroptosis, inflammatory caspases and inflammasomes in infectious diseases. *Immunol Rev* 2017;**277**:61−75.
27. Bai D, Zhou C, Du J, Zhao J, Gu C, Wang Y. TrxR1 is involved in the activation of Caspase-11 by regulating the oxidative-reductive status of Trx-1. *Redox Biol* 2024;**75**:103277.
28. He K, Puebla-Osorio N, Barsoumian HB, Sezen D, Rafiq Z, Riad TS. Novel engineered IL-2 Nemvaleukin alfa combined with PD1 checkpoint blockade enhances the systemic anti-tumor responses of radiation therapy. *J Exp Clin Cancer Res* 2024;**43**:251.
29. Wang S, Liu Y, Xiao H, Chen Z, Yang X, Yin J, et al. Inhibition of SF3B1 improves the immune microenvironment through pyroptosis and synergizes with αPDL1 in ovarian cancer. *Cell Death Dis* 2023;**14**:775.
30. Wang L, Li M, Lian G, Yang S, Wu Y, Cui J. USP18 antagonizes pyroptosis by facilitating selective autophagic degradation of gasdermin D. *Research* 2024;**7**:380.
31. Karunanithi S, Liu R, Hou Y, Gonzalez G, Oldford N, Roe AJ, et al. Thioredoxin reductase is a major regulator of metabolism in leukemia cells. *Oncogene* 2021;**40**:5236−46.
32. Kim MY, Lee H, Ji SY, Kim SY, Hwangbo H, Park S-H, et al. Induction of apoptosis by isoalantolactone in human hepatocellular carcinoma Hep3B cells through activation of the ROS-dependent JNK signaling pathway. *Pharmaceutics* 2021;**13**:1627.
33. Weng Z, Gao H, Hu J, Fan Y, Wang H, Li L. Isoalantolactone induces autophagic cell death in SKOV3 human ovarian carcinoma cells *via* upregulation of PEA-15. *Oncol Rep* 2016;**35**:833−40.
34. Li JK, Jiang XL, Zhang Z, Chen WQ, Peng JJ, Liu B, et al. Isoalantolactone exerts anti-melanoma effects *via* inhibiting PI3K/AKT/mTOR and STAT3 signaling in cell and mouse models. *Phytother Res* 2024;**38**:2800−17.
35. Yin SS, Chen C, Liu Z, Liu SL, Guo JH, Zhang C, et al. Isoalantolactone mediates the degradation of BCR-ABL protein in imatinib-resistant CML cells by down-regulating survivin. *Cell Cycle* 2023;**22**:1407−20.
36. Wang J, Cui L, Feng L, Zhang Z, Song J, Liu D, et al. Isoalantolactone inhibits the migration and invasion of human breast cancer MDA-MB-231 cells *via* suppression of the p38 MAPK/NF-κB signaling pathway. *Oncol Rep* 2016;**36**:1269−76.
37. Chen W, Li P, Liu Y, Yang Y, Ye X, Zhang F, et al. Isoalantolactone induces apoptosis through ROS-mediated ER stress and inhibition of STAT3 in prostate cancer cells. *J Exp Clin Cancer Res* 2018;**37**:309.
38. Jin P, Feng XD, Huang CS, Li J, Wang H, Wang XM, et al. Oxidative stress and cellular senescence: roles in tumor progression and therapeutic opportunities. *MedComm Oncol* 2024;**3**:44−52.
39. Bosman MC, Schuringa JJ, Vellenga E. Constitutive NF-κB activation in AML: causes and treatment strategies. *Crit Rev Oncol Hematol* 2016;**98**:35−44.
40. Kondo K, Shaim H, Thompson PA, Burger JA, Keating M, Estrov Z, et al. Ibrutinib modulates the immunosuppressive CLL microenvironment through STAT3-mediated suppression of regulatory B-cell function and inhibition of the PD-1/PD-L1 pathway. *Leukemia* 2018;**32**:960−70.
41. Nepstad I, Hatfield KJ, Grønningsæter IS, Reikvam H. The PI3K−Akt−mTOR signaling pathway in human acute myeloid leukemia (AML) cells. *Int J Mol Sci* 2020;**21**:2907.
42. Xu Z, Xu J, Sun S, Lin W, Li Y, Lu Q, et al. Mecheliolide elicits ROS-mediated ERS driven immunogenic cell death in hepatocellular carcinoma. *Redox Biol* 2022;**54**:102351.
43. Sun S, Liu H, Shi W, Zhou H, Wu H, Xu W, et al. Protocol for assaying irreversible inhibitors of thioredoxin reductase 1. *STAR Protoc* 2024;**5**:103235.
44. Wang L, Sun S, Liu H, Zhang Q, Meng Y, Sun F, et al. Thioredoxin reductase inhibition and glutathione depletion mediated by glaucocalyxin A promote intracellular disulfide stress in gastric cancer cells. *FEBS J* 2024;**291**:5276−89.
45. Zhang J, Li X, Han X, Liu R, Fang J. Targeting the thioredoxin system for cancer therapy. *Trends Pharmacol Sci* 2017;**38**:794−808.
46. Zhen T, Wu CF, Liu P, Wu HY, Zhou GB, Lu Y, et al. Targeting of AML1-ETO in t(8;21) leukemia by oridonin generates a tumor suppressor-like protein. *Sci Transl Med* 2012;**4**:127ra38.
47. Zhang J, Xu Q, Ma D. Inhibition of thioredoxin reductase by natural anticancer candidate β-lapachone accounts for triggering redox activation-mediated HL-60 cell apoptosis. *Free Radic Biol Med* 2022;**180**:244−52.
48. Glorieux C, Liu S, Trachootham D, Huang P. Targeting ROS in cancer: rationale and strategies. *Nat Rev Drug Discov* 2024;**23**:583−606.
49. Dong C, Zhang NJ, Zhang LJ. Oxidative stress in leukemia and antioxidant treatment. *Chin Med J (Engl)* 2021;**134**:1897−907.
50. Xu S, Liu X, Bao Y, Zhu X, Han C, Zhang P, et al. Constitutive MHC class I molecules negatively regulate TLR-triggered inflammatory responses via the Fps−SHP-2 pathway. *Nat Immunol* 2012;**13**:551−9.
51. Suk FM, Wu CY, Fang CC, Chen TL, Liao YJ. β-HB treatment reverses sorafenib resistance by shifting glycolysis-lactate metabolism in HCC. *Biomed Pharmacother* 2023;**166**:115293.
52. Wu J, Wang H, Gao P, Ouyang S. Pyroptosis: induction and inhibition strategies for immunotherapy of diseases. *Acta Pharm Sin B* 2024;**14**:4195−227.
53. Hu X, Zhao M, Bai M, Xue Z, Wang F, Zhu Z, et al. PARP inhibitor plus radiotherapy reshape the immune suppressive microenvironment and potentiate the efficacy of immune checkpoint inhibitors in tumors with IDH1 mutation. *Cancer Lett* 2024;**586**:216676.
54. Zhang P, Zhang C, Li X, Chang C, Gan C, Ye T, et al. Immunotherapy for gastric cancer: advances and challenges. *MedComm Onco* 2024;**3**:1639487.
55. Yu P, Zhang X, Liu N, Tang L, Peng C, Chen X. Pyroptosis: mechanisms and diseases. *Signal Transduct Targeted Ther* 2021;**6**:128.
56. Choi DC, Tremblay D, Iancu-Rubin C, Mascarenhas J. Programmed cell death-1 pathway inhibition in myeloid malignancies: implications for myeloproliferative neoplasms. *Ann Hematol* 2017;**96**:919−27.
57. Lu LG, Zhou ZL, Wang XY, Liu BY, Lu JY, Liu S, et al. PD-L1 blockade liberates intrinsic antitumourigenic properties of glycolytic macrophages in hepatocellular carcinoma. *Gut* 2022;**71**:2551−60.
58. Pushpakom S, Iorio F, Eyers PA, Escott KJ, Hopper S, Wells A, et al. Drug repurposing: progress, challenges and recommendations. *Nat Rev Drug Discov* 2018;**18**:41−58.
59. Yang Y, Sun S, Xu W, Zhang Y, Yang R, Ma K, et al. Piperlongumine inhibits thioredoxin reductase 1 by targeting selenocysteine residues and sensitizes cancer cells to erastin. *Antioxidants* 2022;**11**:710.
60. Gencheva R, Arnér ESJ. Thioredoxin reductase inhibition for cancer therapy. *Annu Rev Pharmacol Toxicol* 2022;**62**:177−96.

61. Zhang Y, Sun S, Xu W, Yang R, Yang Y, Guo J, et al. Thioredoxin reductase 1 inhibitor shikonin promotes cell necroptosis *via* SecTRAPs generation and oxygen-coupled redox cycling. *Free Radic Biol Med* 2022;**180**:52−62.
62. Yao J, Duan D, Song L, Zhang J, Fang J. Sanguinarine as a new chemical entity of thioredoxin reductase inhibitor to elicit oxidative stress and promote tumor cell apoptosis. *Free Radic Biol Med* 2020;**152**:659−67.
63. Du Z, He Z, Fan J, Huo Y, He B, Wang Y, et al. Au4 cluster inhibits human thioredoxin reductase activity via specifically binding of Au to Cys189. *Nano Today* 2022;**47**:101686.
64. Wen C, Wang H, Wu X, He L, Zhou Q, Wang F, et al. ROS-mediated inactivation of the PI3K/AKT pathway is involved in the antigastric cancer effects of thioredoxin reductase-1 inhibitor chaetocin. *Cell Death Dis* 2019;**10**:809.